TITLE

Single-cell intracellular pH measurements reveal cell-cycle linked pH dynamics

AUTHORS AND AFFILIATIONS

Julia S. Spear[1,2] and Katharine A. White[1,2]

[1]Department of Chemistry and Biochemistry, University of Notre Dame, Notre Dame, IN, USA

[2]Harper Cancer Research Institute, University of Notre Dame, Notre Dame, IN, USA

*to whom correspondence should be addressed: kwhite6@nd.edu

SUMMARY

Spear et al., characterizes an approach for measuring single-cell intracellular pH (pHi) and monitors both single-cell pHi responses to key extracellular signaling cues and pHi dynamics during cell cycle progression. By tracking pHi in single cells, Spear et al. confirms prior work at the population level showing an increase in pHi at the G2/M transition. However, these single-cell pHi measurements reveal new features of pHi dynamics during cell cycle progression, including significantly decreased pHi at the G1/S boundary and rapid acidification during mitosis.

ABSTRACT

Transient changes in intracellular pH (pHi) have been shown to regulate normal cell behaviors like migration and cell-cycle progression, while dysregulated pHi dynamics are a hallmark of cancer. However, little is known about how pHi heterogeneity and dynamics influence population-level measurements or single-cell behaviors. Here, we present and characterize single-cell pHi heterogeneity distributions in both normal and cancer cells and measure dynamic pHi increases in single cells in response to growth factor signaling. Next, we measure pHi dynamics in single cells during cell cycle progression. We determined that single-cell pHi is significantly decreased at the G1/S boundary, increases from S phase to the G2/M transition, rapidly acidifies during mitosis, and recovers in daughter cells. This sinusoidal pattern of pHi dynamics was linked to cell cycle timing regardless of synchronization method. This work confirms prior work at the population level and reveals distinct advantages of single-cell pHi measurements in capturing pHi heterogeneity across a population and dynamics within single cells.

INTRODUCTION

Transient changes in intracellular pH (pHi) regulate normal cell behaviors such as differentiation (Ulmschneider et al., 2016), proliferation (Flinck et al., 2018), migration (Choi et al., 2013), and apoptosis (Sergeeva et al., 2017), and these dynamic changes in pHi result from regulation of ion

transporters that load or extrude protons (Boron, 2004). However, most experiments studying pHi-dependent cell behaviors measure average pHi across a population of cells and in non-native environments. Thus, our understanding of the role of spatiotemporal and single-cell pHi dynamics in regulating cell behaviors is limited. Understanding how spatiotemporal pHi dynamics drive single-cell behaviors like division, migration, and apoptosis would enhance mechanistic understanding of pHi dynamics in regulating cell behaviors. In addition, there is potential to identify new therapeutic routes for limiting pHi-dependent behaviors in disease.

Single cell pHi measurements could be particularly important in studying pHi dynamics in cancer. Cancer cells have a constitutively higher pHi compared to their tissue of origin (0.2-0.4 pHi units) and this has been shown to be an early event in disease progression (Reshkin et al., 2000; Cardone, Casavola and Reshkin, 2005). The alkaline intracellular environment in cancer cells promotes pHi-dependent behaviors that are advantageous to cancer cells, such as proliferation, cell invasion, and metastasis (White, Grillo-Hill and Barber, 2017). Cancer is a disease of clonal evolution and expansion driven by genetic and phenotypic heterogeneity (Greaves and Maley, 2012). Additionally, environmental pressures within a complex tumor microenvironment can enhance and drive phenotypic diversification as cells compete for nutrients, oxygen, and gain fitness advantages for growth and metastasis (Lawson et al., 2018). If pHi correlates with known genetic/phenotypic profiles of cancer cells, then single-cell pHi measurements could predict single-cell behaviors in a heterogenous population. For example, pHi may indicate whether a cell is likely to invade, metastasize, or resist drug treatment during cancer progression. Therefore, there is a critical need to understand how single-cell pHi dynamics regulate single-cell behaviors and determine the effect of single-cell pHi heterogeneity on observed population-level cell behaviors.

Previous work characterizing single-cell pHi has suggested pHi is heterogeneous in cancer cells (Korenchan and Flavell, 2019). In an experiment using the pH-sensitive dye 2',7'-bis(carboxyethyl)-5(6)-Carboxyfluorescein (BCECF), mouse and human cancer cells were shown to have a distribution of pHi values when calculated by fluorescence activated cell sorting (FACS) (Lee and Tannock, 1998). This work suggests that single-cell pHi is heterogeneous in cancer, but the dye was not standardized on the single-cell level and therefore absolute pHi calculations were not possible. In addition, pHi can be rapidly altered when the extracellular environment is changed, as many ion transporters are also mechanosensitive (Fuster, Moe and Hilgemann, 2004; Barth and Fronius, 2019). Therefore, FACS-based single-cell pHi assays cannot reflect the pHi of cells grown under native 2D culture conditions, much less cells in a 3D environment.

A recent study of pHi heterogeneity using 3D spheroid models of cancer and the pH-sensitive dye Seminaphtharhodafluor (SNARF) showed acidic pHi in the hypoxic core (pH 7.0) and alkaline pHi at the spheroid periphery (pH 7.7) (Saccomano et al., 2017). While this suggests that pHi may be reflective of environment or cell phenotype, it is unclear whether this heterogeneity is an artifact of dye penetration issues in large, dense spheroids (>300 μm). In another study using a small number (n<150) of normal and cancerous mouse mammary cells, heterogeneous pHi was linked to metabolic changes (Warburg-like metabolism vs. oxidative phosphorylation) (Lobo et al., 2016). However, the authors did not characterize or quantify heterogeneity within the population of normal or cancer cells, nor did they confirm that single-cell pHi correlated with metabolic phenotype. Collectively, these data suggest that pHi heterogeneity may be a way to distinguish phenotypes, but the lack of single-cell correlations and use of non-native environments limit interpretation of these data.

Here, we present single-cell pHi measurements and characterize pHi heterogeneity distributions in both normal and cancer cells. By measuring the individual pHi of cells grown under

87 physiological conditions in 2D, we show that lung cancer cells have increased pHi in comparison
88 to lung epithelial cells, and that pHi correlates with metastatic potential. We show that pHi is
89 similarly heterogeneous in normal and cancer cell lines, and that we can measure dynamic pHi
90 increases in single cells in response to physiological cues (growth factor signaling). Next, we
91 synchronized cells at two different cell cycle phases and showed dynamic pHi as cells were
92 released, suggesting a link between cell cycle and pHi. Finally, we track single-cell pHi dynamics
93 as cells progress through an entire cell cycle and show trends for pHi dynamics as a marker of
94 cell cycle progression.
95

96 **RESULTS**

97 **Single-cell pHi increases with metastatic potential and heterogeneity is independent of**
98 **transformation**

99 Our first goal was to perform single-cell pHi measurements to quantify pHi distributions within
100 clonal populations of normal and cancerous lung cell lines. We used a genetically-encoded
101 biosensor, mCherry-pHluorin (mCh-pHl), for our applications to avoid issues of uneven dye
102 loading, washout, and photobleaching during time-lapse imaging (Grillo-Hill, Webb and Barber,
103 2014). The mCh-pHl biosensor has previously been used to measure pHi in cultured cells (Choi
104 et al., 2013; Koivusalo et al., 2010) and tissues (Grillo-Hill et al., 2015) and has a dynamic range
105 between pH 6.5 and 8.0 (Grillo-Hill, Webb and Barber, 2014). Briefly, direct measurement of pHi
106 in single living cells can be achieved by performing ratiometric imaging of pHluorin/mCherry
107 fluorescence intensities, as pHluorin is pH-sensitive and mCherry is not, followed by single-cell
108 standardization using buffers of known pH containing the protonophore nigericin (Fig. 1 A, see
109 methods for details).
110

111 We stably expressed mCh-pHl in normal lung epithelial cells (NL20), primary tumor site-derived
112 lung cancer cells (A549), and metastatic site-derived lung cancer cells (H1299). We first

113 confirmed that the average pHi values of the clonal biosensor lines (NL20-mCh-pHl, A549-mCh-
114 pHl and H1299-mCh-pHl) were unchanged compared to matched parental cell lines using a
115 standard population-level plate reader assay with BCECF (Grillo-Hill, Webb and Barber, 2014)
116 (Fig. S1). We next measured single-cell pHi in individual cells across the three biosensor cell lines
117 (Fig. 1, B and D). To quantify heterogeneity in these clonal cell lines, we prepared distribution
118 histograms for single-cell pHi calculations. We found that the normal epithelial cells (NL20-mCh-
119 pHl) had the lowest median pHi (Fig. 1 E; 7.42±0.07), and pHi of the primary tumor cells (A549-
120 mCh-pHl) (Fig. 1 F; 7.54±0.07) was increased compared to normal lung NL20-mCh-pHl cells.
121 Importantly, the H1299-mCh-pHl metastatic tumor cells had the highest median pHi (Fig. 1 G;
122 7.65±0.07), significantly higher than both the normal NL20 and primary tumor A549 cell lines.
123 These data suggest that pHi increases in cancer cells, and higher pHi may correlate with
124 increased metastatic potential.
125

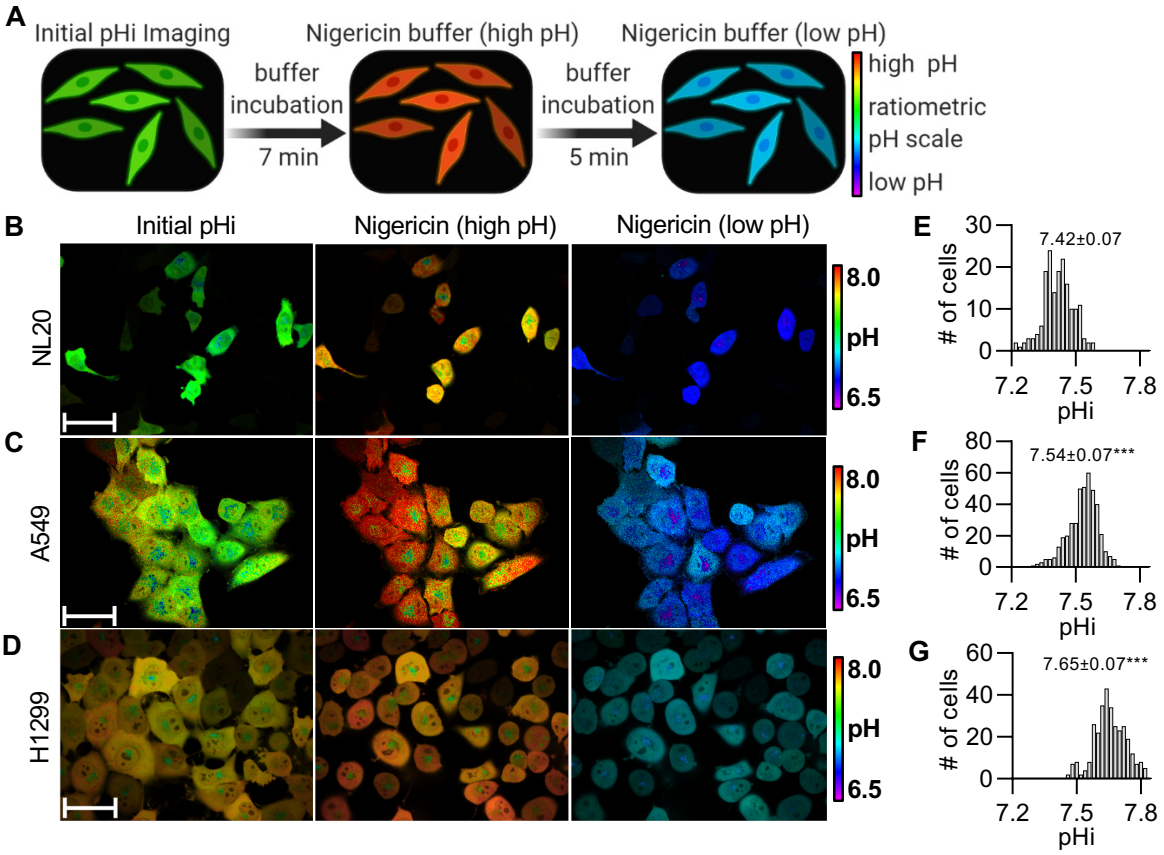

Figure 1: Intracellular pH is heterogenous and varies depending on cell type. A) Schematic of single-cell pHi measurements using a stably expressed pH biosensor, mCherry-pHluorin (mCh-pHl) and the protonophore nigericin to standardize the biosensor (see methods for details). B-D) Representative images of pHi measurement and standardization in NL20 (B), A549 (C) and (D) H1299 cells stably expressing mCh-pHl. Ratiometric display of pHluorin/mCherry fluorescence ratios, scale bars: 50 µm. E-G) Histograms of single-cell pHi in NL20 (E) (n=173, 3 biological replicates), A549 (F) (n=424, 4 biological replicates), and H1299 (G) (n=315, 3 biological replicates). Histograms are binned at 0.02 pH units. Above histograms, median±S.D. Significance was determined by a Mann Whitney test. (***p<0.001, compared to NL20).

It has been proposed that phenotypic heterogeneity may be a key factor in cancer progression in patients (Dagogo-Jack and Shaw, 2018), and it has been shown that cancer cells have increased transcriptional heterogeneity compared to normal cells (Hinohara and Polyak, 2019). We hypothesized that perhaps pHi heterogeneity might be reflective of these other forms of heterogeneity in the framework of metastatic potential. However, we did not see increased pHi heterogeneity in the cancer cell lines compared to the normal lung epithelial lines. Next, we asked

142 whether we could detect physiological fluctuations in single-cell pHi under our culture and imaging
143 conditions.
144
145 **Single-cell pHi increases with growth factor stimulation**
146 Previous work has shown that acute Platelet-Derived Growth Factor (PDGF) stimulation can
147 activate ion transporters involved in pH homeostasis and increase average pHi in a population of
148 cells (Webb et al., 2016). However, we do not know whether PDGF stimulation is sufficient to
149 increase pHi in single cells. To test this, we performed initial pHi imaging of H1299-mCh-pHl cells,
150 then stimulated cells with either PDGF for 5 min (50 ng/mL) or with mock treatment of phosphate
151 buffered saline (PBS) for 5 minutes (Fig. 2 A). We prepared distribution histograms for single-cell
152 pHi calculations and found that with PDGF stimulation, median pHi significantly increased
153 compared to initial (Fig. 2 B, red), while mock-treatment did not result in a significant increase in
154 H1299-mCh-pHl pHi compared to initial measurements (Fig. 2 B, blue). These data suggest that
155 our single-cell pHi measurements can detect physiological changes in pHi and for the first time
156 that growth factor stimulation increases pHi at the single-cell level.
157
158

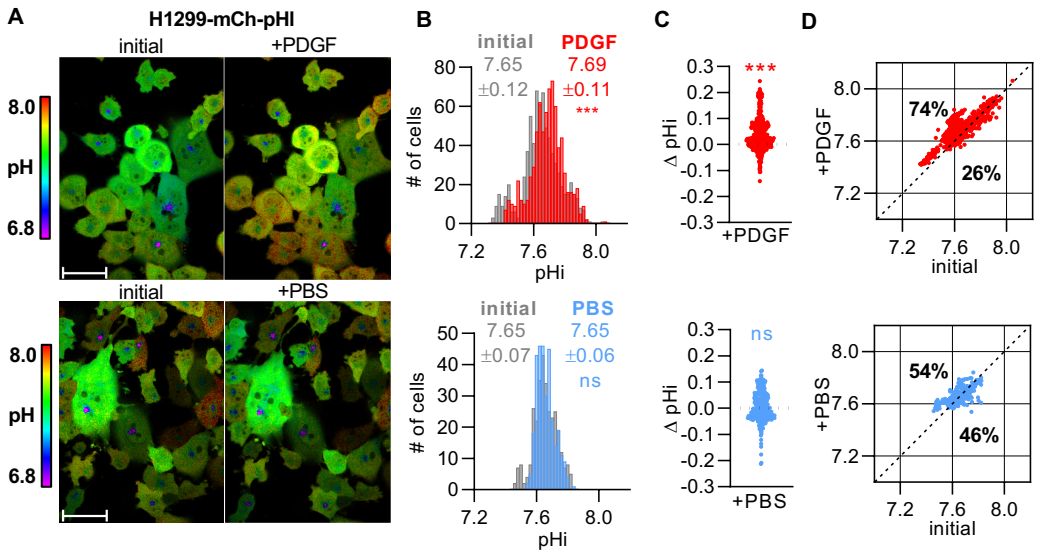

Figure 2: Platelet-Derived growth factor stimulation increased pHi in single H1299-mCh-pHI cells. A) Representative images of H1299-mCh-pHI cells before (initial) and 5 min after stimulation with Platelet-Derived growth factor (+PDGF, 50 ng/mL). Cells subjected to mock treatment with 5 min of PBS (+PBS) are shown below. Ratiometric display of pHluorin/mCherry fluorescence ratios, scale bars: 50 µm. B) Histograms of single-cell pHi data collected as in A, pHi before (grey) and after (red) PDGF stimulation (n=755, 6 biological replicates) or before (grey) and after (blue) mock PBS stimulation (n= 315, 3 biological replicates). Histograms are binned at 0.02 pH units. Above histograms, median±S.D. C) Differences plots showing single-cell pH change (ΔpHi) after PDGF stimulation (red) or mock PBS stimulation (blue). D) Correlation plots comparing initial pH (x-axes) and pH after treatment (y-axes) for PDGF stimulation (red) and mock PBS treatment (blue). Points above identity line represent cells with increased pHi over the experiment while points below line represent cells with decreased pHi over the experiment. Percentage of cells above and below the line are shown. For B, significance was determined by a Wilcoxon test. (***p<0.001). PBS was not significant. For C, significance determined by one-sample Wilcoxon test comparing values to 0. (***p<0.001).

Our single-cell data is in agreement with prior work completed using population measurements (Webb et al., 2016). However, one distinct advantage of our single-cell analyses is the ability to monitor heterogeneity of pHi responses and dynamics within our data. We observed a statistically significant median increase in single-cell pHi with PDGF stimulation (Fig. 2 B), but our data also captured heterogeneous single-cell pHi responses to PDGF (ΔpH = -0.14 to +0.24) (Fig. 2 C, red). While we observed similar heterogeneous responses to PBS treatment (ΔpH = -0.21 to +0.14), PBS did not produce a significant increase in pHi at the single-cell level (Fig. 2 C, blue). Correlation plots in each treatment revealed a higher percentage of cells that increased in pHi in PDGF (74%) when compared to PBS (54%) (Fig. 2 D). These results suggest that growth factor

184 stimulation does increase pHi at the single-cell level, but that this effect is heterogeneous across
185 a population of cells, with some cells responding more strongly than other cells. Importantly,
186 population-level analyses would have missed this heterogenous and physiological response to
187 PDGF.
188
189 To confirm these results, we tested PDGF and mock PBS stimulation in A549-mCh-pHl cells (Fig.
190 S2 A). With this primary tumor line, we saw a small but significant increase with PDGF while PBS
191 stimulation left pHi unchanged (Fig. S2 B). When analyses were performed at the single cell level,
192 pHi responses were significant for PDGF and not significant in PBS (Fig. S2, C and D). Although
193 the magnitude of single-cell pHi changes in A549-mCh-pHl were not as robust as with H1299-
194 mCh-pHl cells in response to PDGF, the data reveal in both cases that PDGF stimulation
195 produces an increase in pHi in single cells but that the response to growth factor is
196 heterogeneous.
197
198 If the initial pHi heterogeneity observed in unstimulated cells were due to differences in phenotype
199 (signaling pathways, crosstalk, metabolic heterogeneity), we would expect that PDGF stimulation
200 would compress the heterogeneity by compressing signaling phenotype. Instead, we saw that pHi
201 heterogeneity was maintained with PDGF stimulation and distributions just shifted slightly to a
202 higher pHi. Furthermore, it is unlikely that the heterogeneity resulted from metabolic or gas
203 exchange differences that have previously been suggested in 3D models (Saccomano et al.,
204 2017), as our system is set up in 2D culture and all cells have the same environmental cues
205 (stiffness, oxygen, nutrient availability). One key feature of the experiments is that they were
206 performed on an asynchronous cell population. There is support for pHi being dynamic during the
207 cell cycle, and there is evidence for pHi as a regulator of cell-cycle progression (Flinck et al.,
208 2018). However, most of this work has been done at a population level, use single-cell model
209 organisms, or use approaches to synchronize cells (like nutrient starvation) which could produce

210 artifactual effects on pHi. We next sought to determine whether cell-cycle heterogeneity is
211 contributing to the measured pHi heterogeneity across all our cell lines.
212
213 **Cells released from G1/S synchronization have dynamic pHi**
214 The first experiments that defined a relationship between cell cycle and pHi used unicellular
215 organisms, such as tetrahymena (Gillies and Deamer, 1979), dictyostelium (Aerts, Durston and
216 Moolenaar, 1985), and *S. pombe* (Karagiannis and Young, 2001). In tetrahymena, two alkaline
217 shifts of 0.4 pH units were observed pre- and post-S phase (Gillies and Deamer, 1979). Starvation
218 and heat shock were used to synchronize the cells, which also alter basic cell metabolic functions
219 and disturb the growth environment, respectively. In dictyostelium, pHi increases (~0.2 pH units)
220 were also measured during S phase, but only population-level pHi was determined (Aerts,
221 Durston and Moolenaar, 1985). In conflict with the previous two studies, no evidence was found
222 for a relationship between cell cycle and pHi in *S. pombe* using genetically-encoded pHluorin
223 (Karagiannis and Young, 2001). Although some key cell functions can be evolutionary conserved
224 from lower-ordered organisms to higher order organisms, pHi fluctuations in unicellular organisms
225 may not be reflective of cell-cycle regulation in multi-cellular organisms.
226
227 More recent work using animal cell models has shown a relationship between pHi and cell cycle
228 progression. Using quiescent populations of human tumor cells, it was shown that a narrow range
229 of extracellular pH (pHe) values (pH 6.8 to 7.2) is required for normal proliferation patterns (Taylor
230 and Hodson, 1984). This work suggests that this defined pHe range can influence both induction
231 of quiescence and recruitment of quiescent cells into the cell cycle, but made no mention of pHi,
232 which can be altered in response to pHe changes (Deutsch, Taylor and Wilson, 1982). In
233 population-level analyses of pHi in thymidine-synchronized MCF-7 breast cancer cells, pHi was
234 found to fluctuate after thymidine release, but no statistical significance was noted (Flinck et al.,
235 2018). Strengthening the link between pHi and cell cycle, knockdown of the Na^+/H^+ exchanger

236 (NHE1) and Na^+-$HCO3^-$ transporter (NBCn1) caused elongation of S phase and a delay in the
237 timing of G2/M transition (Flinck et al., 2018). In another example, an increase in pHi driven by
238 NHE1 was found to time G2/M transition (Putney and Barber, 2003). However, the experiments
239 in these studies were carried out using population-level assays and performed using
240 environmental (pHe change) or ion transporter manipulation. Thus, our understanding of the role
241 of native pHi dynamics on cell cycle progression is incomplete and importantly, physiological
242 single-cell pHi dynamics during cell cycle progression in mammalian models is still
243 uncharacterized.
244
245 With our pHi measurement system using mCh-pHl, we sought to measure single-cell pHi
246 dynamics during cell cycle progression. We synchronized H1299-mCh-pHl using a double-
247 thymidine block (Chen and Deng, 2018) which halts the cells in early S phase. Thymidine acts as
248 a DNA synthesis inhibitor by accumulating dTTP and depleting dCTP within the cell (Bjursell and
249 Reichard, 1973; Bolderson et al., 2004). Once released from the excess thymidine, cells continue
250 through S phase, G2, and eventually enter mitosis (Fig. 3 A). We synchronized H1299-mCh-pHl
251 cells and imaged cells at 0, 4, 8, 12, and 24 hours (h) after thymidine release (Fig. 3 B).
252 Qualitatively, we noticed cells were larger at 0 h and starting at 8 h had distinct cell rounding and
253 smaller apparent cell size, indicating mitotic cells (Fig. 3 B). In this representative replicate, we
254 observed from the single-cell pHi data that pHi significantly decreased between 0 and 4 h,
255 significantly increased between 4 and 8 h, decreased between 8 and 12 h, and increased again
256 between 12 and 24 h (Fig. 3 D). This suggests that following thymidine synchronization release,
257 pHi is dynamic and statistically changes with each time point post release.

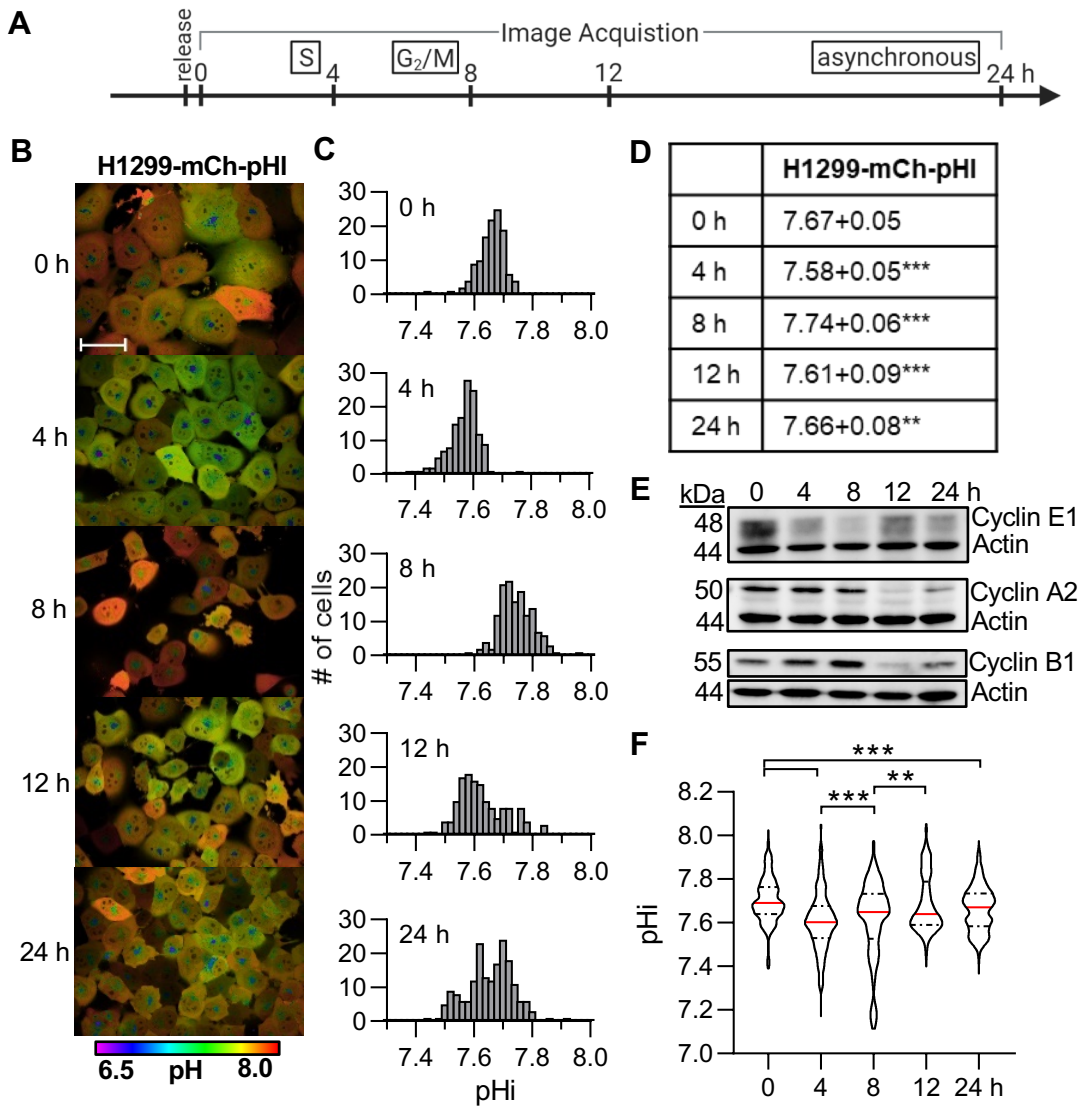

	H1299-mCh-pHI
0 h	7.67+0.05
4 h	7.58+0.05***
8 h	7.74+0.06***
12 h	7.61+0.09***
24 h	7.66+0.08**

Figure 3: Intracellular pH is dynamic after release from G1/S in H1299-mCh-pHI cells and correlates with cyclin levels. A) Schematic of the double-thymidine synchronization protocol. B) Representative images of H1299-mCh-pHI cells at indicated time point after release. Ratiometric display of pHluorin/ mCherry fluorescence ratios, scale bar: 50 µm. C) Histograms of single-cell pHi data collected as in B, from one biological replicate. Histograms binned at 0.02 pH units. D) Table of pHi values from data in C (median±S.D.). E) Representative immunoblots for cyclin E1, A2, and B1 with respective actin loading controls. F) Violin plots of raw pHi across 4 biological replicates. Additional replicates shown in Fig. S3. For D and F, significance was determined using a Kruskal Wallis test with Dunn's multiple comparisons correction. Each time point was compared to its preceding time point and 0 h compared to 24 h. (**p<0.01; ***p<0.001).

269 We confirmed that the double-thymidine block appropriately synchronized the cells by
270 immunoblotting for cyclins from matched cell lysates (Fig. 3 E). Cyclin E1 regulates G1/S (Siu,
271 Rosner and Minella, 2012), cyclin A2 regulates S and G2 phases (De Boer et al., 2008), while
272 cyclin B1 regulates G2 and is degraded by the start of anaphase in mitosis (Chang, Xu and Luo,
273 2003). We observe that cyclin E1, a marker of G1 and early S phase, is highest at 0 h as expected
274 for a cell population properly synchronized at early S phase (Fig. 3 E). These cells undergo mitosis
275 approximately 8 h post-thymidine release since cyclin A2, which is degraded before the G2/M
276 checkpoint, was highest at 4 h and fully degraded at 12 h (Fig. 3 E). Confirming this, we observed
277 that cyclin B1 levels, an inducer of G2/M, increased from 0 to 4 h and peaked at 8 h post-release
278 (G2). Cyclin E1 levels were increasing again by 12 h, suggesting most cells in this assay
279 completed the cell cycle and progress back into G1/S (Fig. 3 E). By 24 h, protein abundance was
280 similar across all cyclins, as we would expect in an asynchronous population. Our cyclin results
281 match previously published data on synchronized H1299 cell populations (Chen and Deng, 2018),
282 suggesting our thymidine protocol is appropriately synchronizing the cells.
283
284 When pHi was compared over four biological replicates, we found that median pHi of the cell
285 populations decreased significantly at 4 h (mid S phase), increased from 4 to 8 h (G2/M), and
286 decreased once more from 8 to 12 h. This preserves the sinusoidal pHi pattern seen in the
287 individual replicate. Individual pHi distribution plots and western blots for additional replicates are
288 shown in Fig. S3. In the merged replicate data, at 24 h there was no significant difference in pHi
289 when compared to 12 h (Fig. 3 F) but was significantly lower than pHi at 0 h. When the
290 synchronized time points (Fig. 3 F, 0-24 h) were compared to our asynchronous time points (Fig.
291 3 F, 24 h; Fig. 1 G) there was no significant difference in pHi (Fig. 3 C). This confirms that
292 thymidine treatment itself did not alter pHi and that merging time points during synchronization
293 reproduces pHi distributions of an asynchronous population. Previous work showed that
294 increased pHi regulates G2/M transition (Putney and Barber, 2003; Sellier et al., 2006). Our data

295 supports this, and in addition reveals a possible role for pHi dynamics in G1/S (where we see a
296 decrease in pHi) and late S phase where pHi increases leading into G2 phase. These pHi values
297 measured from single cells indicate that pHi oscillates after thymidine release and could correlate
298 with different cell-cycle phases.
299
300 A549-mCh-pHI cells were also synchronized with a double-thymidine block and showed similar
301 results post release to H1299-mCh-pHI cells (Fig. 4). Cells were qualitatively similar in
302 appearance to H1299-mCh-pHI populations (Fig. 4 A), and pHi oscillated with cell cycle
303 progression (Fig. 4 B). In the representative replicate shown, the pHi at 4, 8, and 12 h were
304 statistically different from their proceeding time point (Fig. 4 C). These data agree with the pHi
305 oscillations found in H1299-mCh-pHI cells (Fig. 3 D).
306
307 Again, the double-thymidine block synchronization was confirmed by A549-mCh-pHI cyclin
308 immunoblots where peak cyclin A2 (S/G2) was at 4 h and peak cyclin B1 (G2/M) was at 8 h (Fig.
309 4 D). Across four replicates, we observed significant differences in pHi measurements after
310 release, showing an increase from 4h to 8 h (G2/M) and decrease following mitosis at 12 h (G1/S)
311 and 24 h (asynchronous) (Fig. 4 E). Single-cell pHi distribution plots and western blots for
312 additional replicates are shown in Supplementary Fig. 4. This data supports our conclusions made
313 with H1299-mCh-pHI cells (Fig. 3 F) that pHi is dynamic and follows a sinusoidal pattern through
314 cell cycle progression.

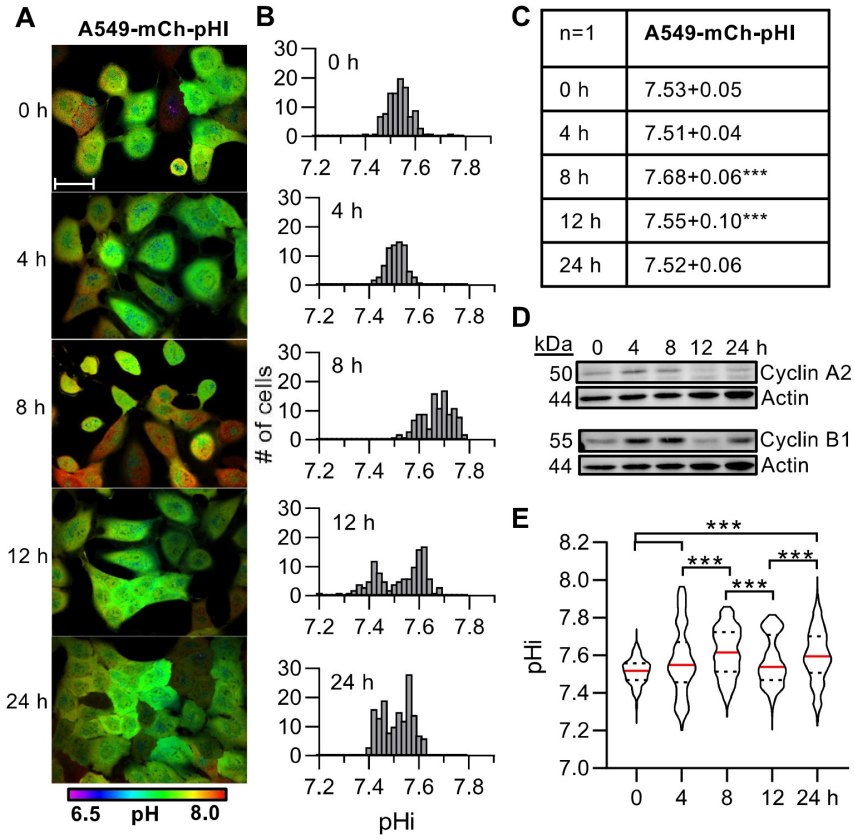

n=1	A549-mCh-pHI
0 h	7.53+0.05
4 h	7.51+0.04
8 h	7.68+0.06***
12 h	7.55+0.10***
24 h	7.52+0.06

Figure 4: Intracellular pH is dynamic after release from G1/S in A549-mCh-pHI cells and correlates with cyclin levels. A) Representative images of A549-mCh-pHI cells at indicated time point after release from a double-thymidine block. Ratiometric display of pHluorin/mCherry fluorescence ratios, scale bars: 50 µm. B) Histograms of single-cell pHi data collected as in A, from one biological replicate. Histograms binned at 0.02 pH units. C) Table of pHi values from data in B, (median±S.D.). D) Representative immunoblots for cyclin E1, A2, and B1 with respective actin loading controls. E) Violin plots of raw pHi across 4 biological replicates. Additional replicates shown in Fig. S4. For C and E, significance was determined using a Kruskal Wallis test with Dunn's multiple comparisons correction. Each time point was compared to the preceding time point and 0 h compared to 24 h. (***p<0.001).

From these cell synchronization data, we conclude that pHi is dynamic following release. Most notably there is a decrease in pHi after release from G1/S, an increase in pHi leading to the G2/M transition, and again a drop in pHi at or following mitosis. We next asked whether pHi dynamics within a single cell tracked over time followed a similar pattern.

331 **Single cells alkalize leading to G2/M, followed by rapid acidification and recovery of**
332 **daughter cells**

333 For the previous experiments, replicates of cell populations were treated and identically released
334 from thymidine, then sampled at distinct time points post release. It is possible that although our
335 time points exemplified pHi distributions that fluctuated in single-cells, the snapshots may not be
336 reflective of continuous single-cell behaviors or of a continuous link between pHi and cell cycle.
337 A time lapse allows us to capture pHi dynamics between time points assayed in our endpoint
338 assay (Fig. 3) and further elucidate single-cell pHi dynamics through an entire cell cycle.
339

340 First, we synchronized H1299-mCh-pHl cells with thymidine as in Fig. 3. Upon release, we imaged
341 cells every 20 minutes for 24 h to acquire dynamic single-cell pHi values. We observed bursts of
342 mitotic cells at 15 h±4 h (3 replicates) indicating cell cycle synchronization. Representative images
343 of a dividing cell from the timelapse are shown, highlighting DNA condensation, cell rounding, and
344 ratiometric changes in the pH biosensor (Fig. 5 A, Video 1). For this cell, pHi quantification shows
345 increasing pHi, acidification just prior to mitosis, and pHi recovery following division in daughter
346 cells (Fig. 5 B). To investigate trends in single-cell pHi dynamics over time, we selected prophase
347 as a “normalization point” for each individual dividing cell. Prophase was chosen because DNA
348 condensation was easily identified using DNA staining. When pHi dynamics were plotted for 39
349 dividing cells, we observed a significant period of alkalization that began ~11 h prior to division
350 and continued until prophase (Fig. 5 C).

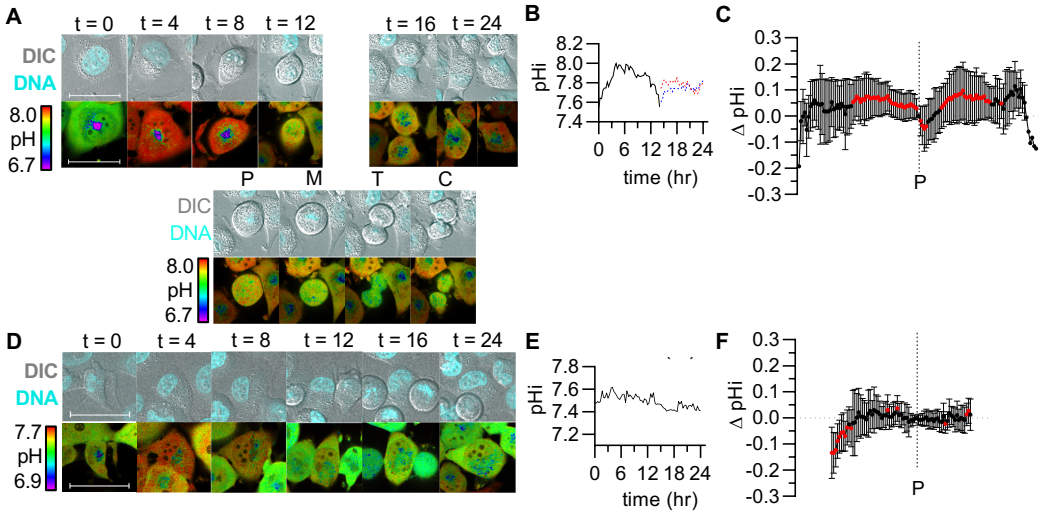

Figure 5: Intracellular pH increases after thymidine release, followed by a rapid acidification leading to division and a recovery of daughter cells. H1299-mCh-pHl cells were synchronized with thymidine and imaged every 20 minutes for 24 h after thymidine release. A) Single Z-plane images of a single cell division at indicated time (h). Top is Hoescht dye (DNA, cyan) and DIC merge. Bottom images are ratiometric display of pHluorin/mCherry fluorescence ratios, scale bars: 50 µm. This dividing cell is shown in Video 1. B) Traces show calculated pHi values of the single cell in A (black, solid line) and daughter cells (red and blue dotted lines). C) Traces show pHi changes in dividing cells, relative to pHi at prophase (P) for each individual cell (mean±SD, n=39, 3 biological replicates). D) Single Z-plane images of a single non-dividing cell. Top is Hoescht dye (DNA, cyan) and DIC merge. Bottom images are ratiometric display of pHluorin/mCherry fluorescence ratios, scale bars: 50 µm. This non-dividing cell is shown in Video 2. E) Traces show calculated pHi values of single cell in D (black, solid line) over time. F) Traces show pHi change in non-dividing cells, relative to the pHi at average time of prophase determined from dividing cell data (meanΔpHi±SD, n=22, from 3 biological replicates). In C, F, significance determined by a one-sample Wilcoxon test compared to 0 (red points, *p<0.05).

This data correlates well with the increased pHi we observe at 8 h (G2/M) in the endpoint pHi measurements (Fig. 3). This sustained increase leading to prophase agrees with previous data on an NHE-1-dependent increase in pHi and the timing of G2/M (Putney and Barber, 2003). Interestingly, the single cell data also reveal a statistically significant acidification following prophase, which may correlate with the acidification observed in the discontinuous H1299-mCh-pHl cells after mitosis (Fig. 3 F, 12h).

374 Although we saw a burst of mitotic cells at an average of 15 h±4 h, there was variability in the
375 timing of prophase (Fig. S5 A), along with pHi heterogeneity noted in single-cell pHi changes from
376 prophase (Fig. S5 B). When dividing cells are binned according to prophase time, significant
377 alkalizations occur in each group pre- and post-prophase (Fig. S5 C). Interestingly at ~5 h prior
378 to prophase, there was a significant alkalization across all groups, indicating that at this distinct
379 time point there may be a requirement for increased pHi for transition to mitosis. (Fig. 5 C). These
380 data suggest that this significant alkalization observed in single-dividing cells correlates with G2/M
381 timing and not with experimental timing.
382
383 Single-cell time-lapse analysis also allows us to differentiate between cells that undergo mitosis
384 and cells that do not. If pHi dynamics are a sufficient regulator of cell cycle progression, we may
385 expect to see attenuated pHi dynamics in non-dividing cells. To test this hypothesis, we also
386 quantified pHi from non-dividing cells in our dataset. A representative non-dividing cell is shown
387 in Fig. 5 D (Video 2). For this cell, pHi quantification showed attenuated pHi dynamics compared
388 to dividing cells (Fig. 5 E). To compare trends in single-cell pHi dynamics for nondividing cells,
389 delta pHi was calculated for each non-dividing cell from the average timing of prophase from
390 dividing cells (15 h) (Fig. 5 F). From the 22 non-dividing cells, we observe attenuated pHi
391 dynamics with the only significant changes coming from a slight period of alkalization just after
392 release (Fig. 5 F). Importantly, the significant alkalization we observe in dividing cells in the ~5
393 hours just prior to G2/M (Fig. 5 C, Fig. S5 C) is not seen in the non-dividers, indicating pHi
394 dynamics could be correlated with (or regulating) mitotic events.
395
396 It is widely accepted that cancer is the culmination of cell cycle dysregulation and the ability of
397 aberrant cells to continue to proliferate (Foster, 2008). On the other hand, it is known that cancer-
398 cell behaviors can be facilitated by dysregulated pHi dynamics (White, Grillo-Hill and Barber,
399 2017). We have shown that after thymidine synchronization, pHi is dynamic and correlates with

400 the cell cycle at the population (Fig. 3) and single-cell level (Fig. 5). Previously it was shown that
401 at a population level, a pHi increase was necessary for G2/M transition (Putney and Barber, 2003;
402 Sellier et al., 2006) and our data supports this. On the single-cell level, pHi alkalization occurs
403 pre-mitosis, followed by a rapid acidification after prophase, and pHi recovery in daughter cells.
404 Our single-cell data uniquely reveals this rapid acidification occurring between prophase and
405 division and subsequent pHi recovery of the daughter cells. Further analysis will be needed to
406 understand if these additional pHi changes are required for a single cell to successfully complete
407 a cell cycle.
408

409 **Cells have similar pHi dynamics independent of cell cycle synchronization timing or**
410 **release**

411 Next, we wanted to independently confirm that pHi dynamics correlate with cell cycle status of a
412 synchronized population. Although thymidine synchronization is a popular method for S phase
413 synchronization, we wanted to see if the measured pHi dynamics we associated with cell-cycle
414 were preserved using synchronization at another phase. Nocodazole can be used after a double
415 thymidine block to push the S-phase-synchronized cells to M phase. However, this approach is
416 technically challenging for adherent cell microscopy, as cells in M phase lose adhesion complexes
417 (Jones, Zha and Humphries, 2019) during rounding and spindle assembly (Taubenberger, Baum
418 and Matthews, 2020). To address this issue, we used a different synchronization method to
419 synchronize the cells at G1 and monitor pHi dynamics in the released cells.
420

421 Palbociclib is a CDK4/6 inhibitor that blocks the phosphorylation of the retinoblastoma protein,
422 which synchronizes cells prior to the G1 checkpoint (Liu, Liu and Chen, 2018) (Fig. 6 A). It has
423 recently been shown that Palbociclib is an efficient G1 synchronizer in H1299 cells, with nearly
424 85% synchronized after 24 h treatment and minimal DNA damage (Trotter and Hagan, 2020). For
425 our experiments, we plated H1299-mCh-pHI cells identically to our double-thymidine block and

426 treated the cells for 24 h with 0.1 μM Palbociclib. After release from Palbociclib treatment, cells
427 were imaged at 0, 4, 8, 12, 24, and 36 h (Fig. 6 B) and single-cell pHi was measured as previously
428 described (Fig. 6 C). As with thymidine synchronization, median pHi was dynamic in H1299-mCh-
429 pHl following Palbociclib release, with pHi significantly changing with each time point post release
430 (Fig. 6 D). We confirmed that Palbociclib synchronized the cells by immunoblotting for cyclins
431 from matched cell lysates (Fig. 6 E). Notably we see a significant delay in G2/M with Palbociclib
432 compared to thymidine, as cyclin A2 (G2 marker) peaks at 12 h with Palbociclib (4 h with
433 thymidine) and cyclin B1 (G2/M marker) peaks at 24 h with Palbociclib (8 h with thymidine) (Fig.
434 6 E). Additional western blot replicates are shown in Fig. S6 B. This suggests that S phase may
435 be elongated or entry into G2 may be delayed with Palbociclib compared to thymidine, but that
436 our experimental assay is still capturing progression through a full cell cycle.

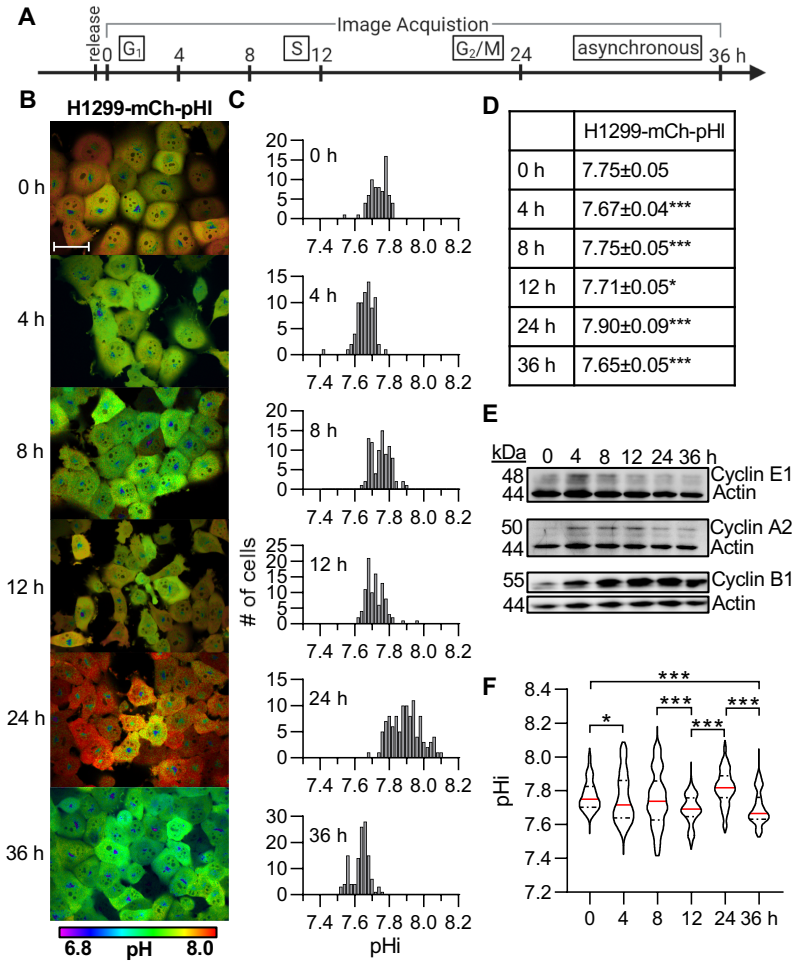

	H1299-mCh-pHI
0 h	7.75±0.05
4 h	7.67±0.04***
8 h	7.75±0.05***
12 h	7.71±0.05*
24 h	7.90±0.09***
36 h	7.65±0.05***

Figure 6: Intracellular pH is dynamic following G1 synchronization and pHi heterogeneity increases with time post-release. A) Schematic of Palbociclib synchronization protocol. B) Representative images of H1299-mCh-pHI cells at indicated time point after release. Ratiometric display of pHluorin/mCherry fluorescence ratios. Scale bar: 50 µm. C) Histograms of single-cell pHi data collected as in B, from one biological replicate. Histograms binned at 0.02 pH units. Additional replicates shown in Fig. S6. D) Medians and standard deviations at each time point shown in C. E) Representative immunoblots for cyclin E1, A2, and B1 with respective actin loading controls. F) Violin plots of raw pHi across 4 biological replicates. Additional replicates shown in Fig. S6. Significance in D and F was determined according to a Kruskal Wallis test with Dunn's multiple comparisons correction. Each time point was compared to its preceding time point. (*p<0.05; ***p<0.001).

When pHi measurements on Palbociclib-treated cells were compared over three biological replicates, we found that pHi decreased at mid-S phase (12 h, 7.69±0.09) and increased at G2/M (24 h, 7.82±0.11) (Fig. 6 F). At 36 h, pHi significantly decreased (36 h, 7.67±0.10), but was still

452 significantly higher than asynchronous pHi (Fig. 6 C). However, even with the uniform increase in
453 resting pHi, our data suggests a consistent link between pHi dynamics and cell cycle, with
454 decreasing pHi in early-to-mid-S and increasing pHi in late S leading up to G2/M.
455
456 To better compare and correlate pHi fluctuations in both thymidine and Palbociclib data, which
457 have differential effects on cell cycle timing in H1299, we used cyclin quantification to match pHi
458 data to cell cycle. As mentioned previously, cyclin E1 regulates G1/S (Siu, Rosner and Minella,
459 2012), cyclin A2 regulates S and G2 phase (De Boer et al., 2008), while cyclin B1 regulates G2
460 and is degraded by the start of anaphase (Chang, Xu and Luo, 2003) (Fig. 7 A). After
461 quantification of cyclin levels across our data (Fig. 7, B and C), we determined that cyclin E1
462 (G1/S phase) would be the most reliable marker to align our data so that we can directly compare
463 pHi changes between the two treatments. When ΔpHi was calculated from the median pHi at 0 h
464 (thymidine) and 4 h (Palbociclib), we found that in both treatments pHi decreased after the G1/S
465 boundary (Fig. 7 D; pink) into S/G2 phase (Fig. 7 D; green). For Palbociclib-treated cells, we found
466 sustained increase of cyclin A2 and steady increase of cyclin B1, suggesting an elongated S/G2
467 phase in Palbociclib compared to thymidine. The pHi corresponding to the latter end of the
468 elongation was decreased compared to the flanking time points (in G1/S and G2/M). Next, there
469 was a significant increase in pHi when G2/M would be occurring, determined by high cyclin B1
470 expression (Fig. 7 D; purple). In thymidine-treated cells, we were able to measure a decrease in
471 pHi at G1 phase, represented by an increase in cyclin E1 at 12 h (Fig. 7 B; 7 D, black).
472 Asynchronous populations returned to resting pHi for thymidine-treated cells or near resting pHi
473 for Palbociclib-treated cells (Fig. 7 D, blue; Fig. S3 C; 6 C).

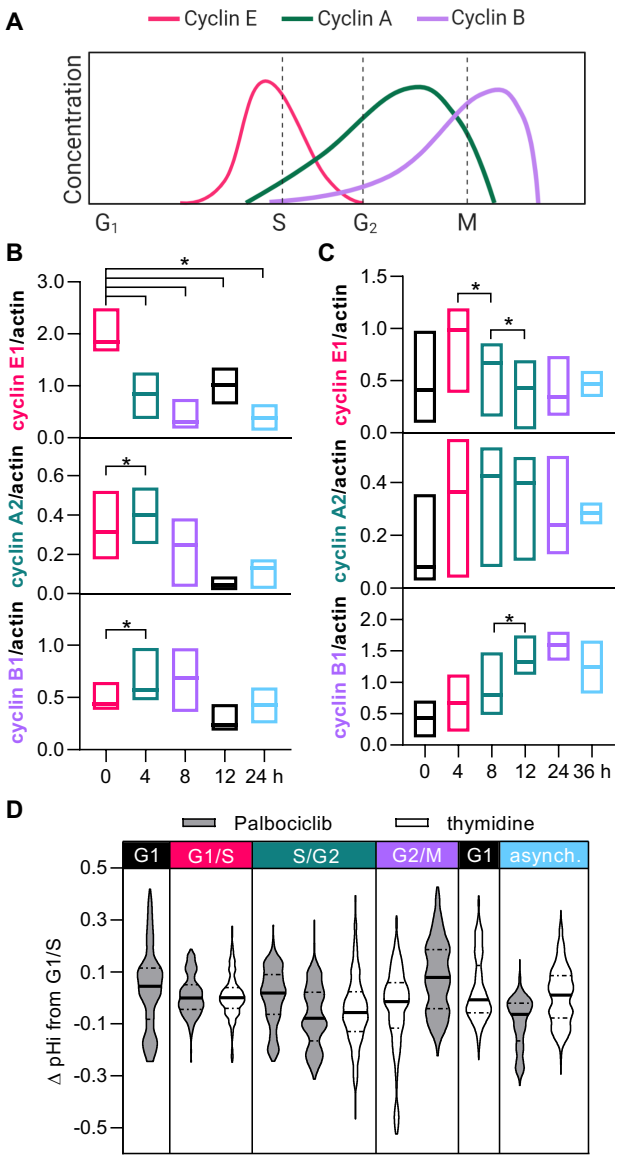

474 **Figure 7: Intracellular pH fluctuations correlate with cyclin concentrations independent of**
475 **synchronization time.** A) Schematic of Cyclin concentration during the cell cycle (adapted from
476 BioRender). Quantification of H1299-mCh-pHl cyclin immunoblots after B) thymidine release (Fig.
477 3 E and Fig. S3, n=4) and after C) Palbociclib release [(Fig. 6 E, Fig. S6; n=3 (0-24 h), n=2 (36
478 h)] normalized to actin within each replicate. C) Violin plots of single-cell delta pHi from peak cyclin
479 E1 concentration (thymidine, 0 h; Palbociclib, 4 h) across 4 (thymidine) and 3 (Palbociclib)
480 biological replicates. Data is reproduced from Fig. 3, 6, S3 and S6. For B and C, significance was
481 determined according to a paired t-test, two-tailed. Each time point was compared to its preceding
482 time point. (*p<0.05).
483

484 In these two treatment conditions to synchronize cells at different points in the cell cycle, we were

485 able to conclude that pHi oscillates according to cell cycle progression when correlated with peak

486 cyclin expression, further supporting a pHi and cell cycle link. In addition, our data suggest that
487 pHi may be an predictor or regulator of cell cycle phase, as pHi has previously been shown to
488 regulate G2/M (Putney and Barber, 2003; Sellier et al., 2006) and it is possible that the decreases
489 we see after G1 and during mitosis may also be predicative or regulating cell cycle progression.
490 In summary, our single-cell measurements, both via time points and time lapse, show novel pHi
491 dynamics and support the idea that pHi may be more indicative of basic and necessary cell
492 function.
493

494 **DISCUSSION**

495 Intracellular pHi dynamics have been implicated in diverse cellular processes like differentiation
496 (Ulmschneider et al., 2016), proliferation (Flinck et al., 2018), migration (Choi et al., 2013), and
497 apoptosis (Sergeeva et al., 2017). However, our mechanistic understanding of the role of
498 spatiotemporal and single-cell pHi dynamics in regulating cell behaviors is limited. This is partially
499 due to reliance on population analyses, non-physiological environments, or genetic alteration to
500 link pHi and phenotype (Czowski et al., 2020).
501

502 Here, we present three key results that link single-cell pHi and non-genetic phenotype. First, our
503 single-cell pHi measurements confirm pHi is heterogeneous even in clonal cell lines, suggesting
504 pHi may correlate with non-genetic phenotypic variation. Second, we confirmed using single-cell
505 approaches that transformed cells have a higher median pHi compared to normal cells, agreeing
506 with population-level analyses that suggest cancer cells have an increased pHi setpoint compared
507 to normal cells (White, Grillo-Hill and Barber, 2017). However, our single-cell analysis reveals that
508 pHi heterogeneity is similar when compared across normal and transformed cell lines. This result
509 was surprising, as we hypothesized that pHi may be reflective of the increased heterogeneity in
510 cancer (Hinohara and Polyak, 2019). Third, we showed that we can measure physiological
511 increases in single-cell pHi in response to growth factor stimulation (PDGF). Our single-cell

512 analysis revealed heterogeneous increases in pHi in response to growth factor stimulation. Future
513 work focused on correlating PDGF pathway activation heterogeneity and pHi response
514 heterogeneity would strengthen the link between pHi and cell-signaling phenotype. Taken
515 together, our single-cell pHi and PDGF stimulation measurements suggest that pHi may be a
516 marker of underlying cell phenotype. This motivates testing whether pHi can be a potential
517 biomarker of more cryptic phenotypic markers such as cell cycle status, metabolic activity, and
518 differentiation.
519
520 As proof of concept for a pHi-phenotype link, we tested whether pHi heterogeneity is linked to cell
521 cycle. Prior work has suggested a role for pHi in regulating G2/M transition (Putney and Barber,
522 2003), but several papers show conflicting results with no temporal correlation of pHi and cell-
523 cycle at the population level (Aerts et al., 1985; Flinck et al., 2018; Gillies & Deamer, 1979;
524 Karagiannis & Young, 2001; Putney & Barber, 2003; Taylor & Hodson, 1984).
525
526 Here, we present two key results that suggest a link between cell cycle and pHi at both the
527 population and single-cell levels. First, we show that at a population level, H1299-mCh-pHl cell
528 pHi is significantly decreased after the G1/S boundary, increases throughout S phase and peaks
529 just prior to G2/M. This was true using two techniques to synchronize cells at different stages of
530 the cell cycle. We also confirmed the increase leading to the G2/M transition in multiple cell lines.
531 Second, we show that single-cell pHi dynamics follow a sinusoidal curve over the cell cycle, with
532 pHi increasing through S phase, peaking at G2/M and dropping during mitosis before recovering
533 in daughter cells. This has mechanistic implications for prior work showing pHi gradients
534 generated in morphogenetic tissues where bursts of synchronized cell proliferation may underlie
535 these observations (Weiß and Bohrmann, 2019). More work is needed to determine whether
536 these pHi dynamics are necessary or sufficient drivers of cell division or cell cycle progression at

537 the single-cell level and identify the pH-sensitive proteins that mediate pHi-dependent cell cycle
538 progression.
539
540 The impact of this work shows that single-cell techniques can elucidate detailed maps of single-
541 cell behaviors and heterogeneity that can be correlated with population analysis. However, single-
542 cell approaches also reveal dynamics that are not detectable at the population level. The single-
543 cell pHi dynamics reported here in response to growth factor signaling and cell cycle changes
544 could be critical for understanding complex cell biology integrating single-cell and tissue-level
545 behaviors. This is particularly true for understanding pHi-dependent behaviors in the context of
546 cancer, where cell-intrinsic genetic and phenotypic heterogeneity integrate with complex
547 microenvironment features to drive single-cell resistance or metastasis phenotypes. Future work
548 on heterogeneity within complex environments is needed to fully understand how pHi may
549 correlate with cancer-related behaviors and whether pHi can be predicative of cell phenotype.
550

551 **MATERIALS AND METHODS**

552 **Cell culture and conditions**

553 Complete media for H1299 cells (ATCC CRL-5803): RPMI 1640 (Corning, 10-040-CV)
554 supplemented with 10% Fetal Bovine Serum (FBS, Peak Serum, PS-FB2); A549 (ATCC CCL-
555 185): DMEM (Corning, MT10013CVV) supplemented with 10% FBS; and NL20 (ATCC CRL-
556 2503): Ham's F12 (Lonza, 12001-578) supplemented with 4% FBS, 1.5 g/L sodium bicarbonate
557 (Sigma, S6014), 2.7 g/L glucose (VWR, BDH9230), 2.0 mM Glutamax (Gibco, 35050079), 0.1
558 mM nonessential amino acids (Lonza, BW13114E), 0.005 mg/mL insulin (Sigma, I1882), 10
559 ng/mL EGF (Peprotech, AF-100-15), 0.001 mg/mL transferrin (BioVision, 10835-642), 0.0005
560 mg/mL hydrocortisone (Sigma, H0888). All cells were maintained at 5% CO_2 and 37°C in a
561 humidified incubator.
562

563 **Transfections and stable cell line selection**

564 H1299 cells were transfected with the pCDNA3-mCherry-SEpHluorin(Mirkka Koivusalo,
565 Christopher Welch, Hisayoshi Hayashi, Cameron C. Scott, Moshe Kim, Todd Alexander, Nicolas
566 Touret, Klaus M. Hahn, 2010) (mCh-pHl) using Lipofectamine2000 (Life Technologies, 11668019)
567 per manufacturer's instructions. After 24 h, cells were trypsinized and plated at low dilution on a
568 10 cm dish in media containing 0.8 mg/mL Geneticin. Cloning cylinders were used to select
569 colonies expressing mCh-pHl for expansion. A final clone was selected based on microscopy
570 assay for mCh-pHl expression and comparison of cell morphology and pHi to parental H1299.

571

572 Lentiviral transfection was used to generate stable mCherry-pHluorin expression in NL20 and
573 A549 cells. Production of virus was carried out in 293FT cells. Cells were grown to near
574 confluency in a 10 cm dish and transfected with plx304-mCherry-SEpHluorin (Gift of Yi Liu and
575 Diane Barber at UCSF) and two packaging plasmids: PSPAX2 (Addgene #12260) and PMD2.6
576 (Addgene #12259) provided by Siyuan Zhang (University of Notre Dame). Three µg each of the
577 plx304-mCherry-pHluorin, PSPAX2, and PDM2.6 were transfected into a nearly confluent 10 cm
578 dish of 293FT cells using Lipofectamine2000 for 18 h. Media was changed and incubated another
579 3 days. Viral supernatant was collected from the cells and centrifuged for 15 min at 3000 rpm.
580 Supernatant was passed through a 0.2 µm polyethersulfone filter, flash frozen in liquid nitrogen
581 in 1 mL aliquots, and stored at -80°C.

582

583 For viral transduction, NL20 and A549 cells were plated in a 6-well plate. After 24 h, viral
584 supernatant was diluted 1:1.6, 1:3 and 1:10 into antibiotic-free media (depending on cell line) with
585 10 µg/mL Polybrene (Sigma, TR-1003-G), added to separate wells, and incubated for 48-72 hr.
586 Transduced cells were moved to a 10 cm dish and selected with 5 µg/mL blasticidin (Fisher,
587 BP264725). NL20 cells were plated at low density in 96 well plates (0.5 cells/well). Colonies
588 expressing mCh-pHl were expanded and a final NL20-mCh-pHl clone was chosen based on

589 microscopy assay for mCh-pHI expression and comparison to morphology and pHi of
590 parentals. A549 cells were sorted using fluorescence-activated cell sorting (FACS) and a
591 population sort according to mCherry expression was used for all imaging experiments after
592 confirmation with microscopy.
593
594 **BCECF plate reader assays**
595 Cells were plated at $4.0x10^5$ - $8.0x10^5$ cells/well in a 24-well plate. 24 h later, cells were treated
596 with 2 μM 2',7'-Bis-(2-Carboxyethyl)-5-(and-6)-Carboxyfluorescein, Acetoxymethyl Ester
597 (BCECF-AM) (VWR, 89139-244) for 30 min at 37°C and 5% CO_2. Cells were washed 3x5 minutes
598 with a pre-warmed (37°C) HEPES-based wash buffer (30 mM HEPES pH 7.4, 145 mM NaCl, 5
599 mM KCl, 10 mM glucose, 1 mM $MgSO_4$, 1 mM $KHPO_4$, 2 mM $CaCl_2$, pH 7.4) for NL20 and H1299
600 cells or a pre-warmed (37°C) Bicarbonate (HCO_3)-based wash buffer (25 mM HCO_3, 115 mM
601 NaCl, 5 mM KCl, 10 mM glucose, 1 mM $MgSO_4$, 1 mM $KHPO_4$, 2 mM $CaCl_2$, pH 7.4). Two
602 Nigericin buffers (25 mM HEPES, 105 mM KCl, 1 mM $MgCl_2$) supplemented with 10 μM Nigericin
603 (Fisher, N1495) and pH adjusted to ~6.7 and ~7.7 were also prepared and pre-warmed to 37°C.
604 Fluorescence was read (ex 440, em 535; ex 490, em 535) on a Cytation 5 plater reader incubated
605 at 37°C with 5% CO_2. Kinetic reads were taken at 15 sec intervals for 5 min, using protocol
606 established within Gen5 software. After initial pHi read, the HEPES/bicarbonate wash was
607 aspirated and replaced with one of the nigericin buffer standards, incubated at 37°C with 5% CO_2
608 for 7 min, then BCECF fluorescence was read by plate reader as above. This process was
609 repeated with the second nigericin standard. Mean intensity ratio (490/440) was derived from
610 each read. Measurements were calculated from a nigericin linear regression using exact nigericin
611 buffer pH to hundredths place.(Grillo-Hill, Webb and Barber, 2014)
612
613
614

615 **Microscopy**

616 Imaging protocol was derived from Grillo-Hill et al.[2] Cells were plated on a 35 mm imaging dish
617 with a 14 mm glass coverslip (Matsunami, D35-14-1.5-U) a day prior to imaging. Microscope was
618 preheated to 37°C and kept at 5% CO_2/95% air. Confocal images were collected on a Nikon Ti-2
619 spinning disk confocal with a 40x (CFI PLAN FLUOR NA1.3) oil immersion objective. The
620 microscope is equipped with a stage-top incubator (Tokai Hit), a Yokogawa spinning disk confocal
621 head (CSU-X1), four laser lines (405nm, 488nm, 561 nm, 647 nm), a Ti2-S-SE motorized stage,
622 multi-point perfect focus system, and an Orca Flash 4.0 CMOS camera. Hoescht dye (405 laser
623 ex, 455/50 em), pHluorin (488 laser ex, 525/36 em), mCherry (561 laser ex, 605/52 em).
624 Acquisition times for each fluorescence acquisition ranged from 100-800 milliseconds.

625

626 For imaging, Initial fields of view (FOV) were collected on the cells in their respective media. For
627 all imaging, nigericin buffers were prepared identically to BCECF assays and all buffer exchanges
628 were carried out on the stage incubator to preserve XY positioning. Multiple Z-planes were
629 collected with center focal plane maintained using a Perfect Focus System (PFS).

630

631 After acquisition, NIS Analysis Software was used to quantify pHi. Images were background
632 subtracted using an ROI drawn on glass coverslip (determined by DIC). Individual Regions of
633 Interest (ROI) are drawn for each cell in each condition (initial, stimulation, high pH nigericin, and
634 low pH nigericin). For each cell ROI, mean pHluorin and mCherry pixel intensities were quantified,
635 and pHluorin/mCherry ratios calculated in excel. For each cell, nigericin values were used to
636 generate a standard curve and pHi was back-calculated from the single-cell standard curve.

637

638 **PDGF stimulation**

639 For Fig. 2, cells were stimulated with 50 ng/mL Platelet-Derived Growth Factor (PDGF)
640 (Peprotech, 100-00AB) or 2 µL PBS used as a negative control and second images were collected

641 5 min after PDGF addition on the same FOV of cells collected initially. PBS was used as a control,
642 using 2 μL and collecting images 5 min after addition.
643
644 **Double-thymidine block**
645 Cells were plated at 10% confluency in 5 replicate 35 mm glass-bottomed dishes and 5 6-well
646 plates (for protein lysate collection) and incubated overnight. Dishes were identically treated with
647 2 mM Thymidine (Sigma, T9250) for 18 hr, washed with PBS and incubated with fresh complete
648 media for 9 hr, then treated for another 18 h with 2 mM thymidine. Cells were released with a PBS
649 wash and fresh complete media. Imaging of the 0 h time point was initiated 20 min after release.
650 Subsequent imaging was collected at 4, 8, 12, and 24 h after release. Matched dishes at each
651 time point were washed twice with PBS and frozen at -80°C for protein lysate collection and
652 immunoblot analysis of cyclins.
653
654 For time-lapse imaging, the double-thymidine block was used as explained above on a single 35
655 mm glass-bottomed dish supplemented with 1% Pen/Strep (Corning, 30-001-C1) to avoid
656 bacterial contamination during long-term acquisition. Hoechst 33342 solution (ThermoFisher,
657 62249) was added to the cells (1:20,000) before release and incubated for 15 min. Dye and
658 thymidine were removed and cells were washed with PBS to release cells. Fresh media was
659 added and images were collected every 20 min for 24 hr. Optimal acquisition parameters were
660 as follows: 700 ms exposure time and 8% laser power for GFP; 700 ms exposure time and 10%
661 laser power for TxRed; and 100 ms exposure time and 5% laser power DAPI. A single Z-plane
662 was collected to avoid excess light. Nigericin standards were carried out as previously described
663 (Grillo-Hill, Webb and Barber, 2014).
664
665
666

667 **Palbociclib synchronization**

668 Cells were plated at 10% confluency in 5 replicate 35 mm glass-bottomed dishes and 5 6-well
669 plates (for protein lysate collection) and incubated overnight. Dishes were identically treated with
670 0.1 μM Palbociclib (PD-0332991) (Selleck, S1116) for 24 h. Cells were washed with PBS and
671 released with complete fresh media. Imaging of the 0 h time point was initiated 20 min after
672 release. Subsequent imaging was collected at 4, 8, 12, 24 and 36 h post release (1 replicate 0-
673 24 h, 2 replicates 0-36 h). Matched dishes at each time point were washed twice with PBS and
674 frozen at -80°C for later protein lysate collection and immunoblot analysis of cyclins.

675

676 **Western blot**

677 Protein lysates were collected from 35-mm dishes or 6-well plates frozen at time points matched
678 to imaging. Ice-cold lysis buffer [50 mM TRIS, 150 mM NaCl, 1 mM dithiothreitol (DTT), 1 mM
679 Ethylenediaminetetraacetic acid (EDTA), 1% Triton X-100, Roche Protease Inhibitor Cocktail]
680 was added to the samples and incubated for 15 min on ice. Cells were scraped and centrifuged
681 for 10 min at 13,000 g at 4°C. Supernatant was retained and protein concentration determined by
682 Pierce™ BCA (ThermoFisher, 23225) protein assay.

683

684 15 μg protein was loaded onto an SDS- Polyacrylamide gel electrophoresis (PAGE) was run for
685 3 h at 120 V in 1X Tris-glycine (3.02 g/L Tris, 14.4 g/L glycine, 1.0 g/L SDS). Either a wet-transfer
686 system or a Trans-Blot Turbo Transfer System (Bio-Rad) was used to transfer the proteins to a
687 polyvinylidene fluoride (PDVF) membrane (pre-wet with methanol). For the wet-transfer, 1X
688 transfer buffer (141 g/L Glycine, 0.3 g/L Tris base) with 20% Methanol for 1.5 h at 100 V. For the
689 Trans-Blot Turbo Transfer, Bio-Rad transfer buffer was used according to manufacturer's protocol
690 (7 min). Membranes were blocked in 5% BSA in TBST (2.42 g/L Tris, 8 g/L NaCl, 0.1% Tween)
691 for 2 h then divided for blotting. Primary antibodies: α-cyclin A2 (1:500; abcam, ab38), α-cyclin B1
692 (1:1,000; Cell Signaling, 12231), α-cyclin E1 (1:1000; Cell Signaling, 4129) actin (1:1,000; Santa

693 Cruz, 2Q1055). Membranes were incubated with primary antibody solution overnight at 4°C with
694 shaking (4 h at RT with shaking for actin). Membranes were washed 3x10 min TBST at RT with
695 shaking and incubated with secondary antibodies [1:10,000; goat α-mouse IgG HRP (Bio-Rad,
696 1721011) or goat α-rabbit IgG HRP (Bio-Rad, 1706515)] for 2 h at RT with shaking. Membranes
697 were washed 3x10 min TBST at RT with shaking, developed using SuperSignal™ West Pico
698 PLUS Chemiluminescent Substrate (ThermoFisher, 34578), and visualized using a ChemiDoc
699 MP Imaging System (BioRad). ImageJ was used for protein quantification, normalized to loading
700 control.
701
702 **Quantification and statistics**
703 GraphPad Prism was used to prepare graphs and perform statistical analyses. Normality tests
704 were performed on all data sets, along with an outlier test using ROUT method (Q=1%). For
705 normal data, an unpaired t-test (Fig. S1) or paired t-test (Fig. 7, B and C) was used. For non-
706 normal, unpaired data (Fig. 1, E and G; S1 B; 3 C; 6 C), a Mann Whitney test was used. For non-
707 normal, paired data (Fig. 2 B; S2 B), a Wilcoxon test was used. For differences plots (Fig. 3 C;
708 S2 C) and time lapse data (Fig. 5 C; 5 F; S5 C), a one-sample Wilcoxon test was used, compared
709 to a theoretical mean of 0. For non-normal, unpaired data with more than two sets, a Kruskal-
710 Wallis test with Dunn's multiple comparisons test was used (Fig. 3 D; 3 F; 4 C; 4 E; 6 D; 6 F; S3
711 A, S4 A, S6 A). Values were binned at 0.02 in all frequency distributions. All significance was
712 determined by the following: *$p<0.05$; **$p<0.01$; ***$p<0.001$.
713
714 **Online supplemental material**
715 Fig. S1 shows that the stable mCherry-pHluorin biosensor expression does not alter pHi
716 compared to parental cell lines. Fig. S2 shows that Platelet-Derived growth factor stimulation
717 increased pHi in single A549-mCh-pHl cells. Fig. S3 shows additional replicates of Fig. 3, where
718 single-cell pHi was dynamic after release from G1/S in H1299-mCh-pHl cells. Fig. S4 shows

719 additional replicates of Fig. 4, where single-cell pHi was dynamic after release from G1/S in A549-
720 mCh-pHl cells. Fig. S5 illustrates heterogenous timing of prophase but preserved pHi changes
721 from time lapse experiments shown in Fig. 5. Fig. S6 shows additional replicates of Fig. 6, where
722 single-cell pHi was dynamic after release from G1 in H1299-mCh-pHl cells. Video 1 is derived
723 from Fig. 5 A and B and demonstrates that pHi of a dividing cell is dynamic following release from
724 G1/S. Video 2 is derived from Fig. 5 D and E and demonstrates that pHi dynamics of a non-
725 dividing cell are attenuated following release from G1/S.
726

727 **ACKNOWLEDGEMENTS**

728 We would like to thank Dr. Siyuan Zhang and Dr. Diane Barber for plasmids. We would also like
729 to thank members of the White lab for their helpful feedback on the manuscript.
730 This work was supported by a DP2 (1DP2CA260416-01) to K.A.W.
731 The authors declare no competing financial interests.
732

733 **AUTHOR CONTRIBUTIONS**

734 K. White conceptualized the initial hypothesis, developed in collaboration with J. Spear. J. Spear
735 collected and analyzed all data in consultation with K. White. J. Spear wrote initial draft of the
736 manuscript, which was revised in collaboration with K. White. Both authors contributed to figure
737 preparation and approved final manuscript for submission.
738

739 **REFERENCES**

740 Aerts, R. J., Durston, A. J., & Moolenaar, W. H. (1985). Cytoplasmic pH and the regulation of the
741 dictyostelium cell cycle. *Cell*, *43*(3 PART 2), 653–657. https://doi.org/10.1016/0092-
742 8674(85)90237-5

743 Barth, D., & Fronius, M. (2019). Shear force modulates the activity of acid-sensing ion channels
744 at low pH or in the presence of non-proton ligands. *Scientific Reports*, *9*(1).
745 https://doi.org/10.1038/s41598-019-43097-7
746 Bjursell, G., & Reichard, P. (1973). Effects of thymidine on deoxyribonucleoside triphosphate
747 pools and deoxyribonucleic acid synthesis in Chinese hamster ovary cells. *Journal of*
748 *Biological Chemistry*, *248*(11), 3904–3909. https://doi.org/https://doi.org/10.1016/S0021-
749 9258(19)43819-2
750 Bolderson, E., Scorah, J., Helleday, T., Smythe, C., & Meuth, M. (2004). ATM is required for the
751 cellular response to thymidine induced replication fork stress. *Human Molecular Genetics*,
752 *13*(23), 2937–2945. https://doi.org/10.1093/hmg/ddh316
753 Boron, W. F. (2004). Regulation of intracellular pH. *American Journal of Physiology - Advances*
754 *in Physiology Education*, *28*(4), 160–179. https://doi.org/10.1152/advan.00045.2004
755 Bryne Ulmschneider, Bree K. Grillo-Hill, Marimar Benitez, Dinara R. Azimova, D. L. B. and T. G.
756 N. (2016). Increased intracellular pH is necessary for adult epithelial and embryonic stem
757 cell differentiation. *Journal of Cell Biology*, *215*(3), 345–355.
758 https://doi.org/10.1083/jcb.201606042
759 Cardone, R. A., Casavola, V., & Reshkin, S. J. (2005). The role of disturbed pH dynamics and the
760 NA+/H+ exchanger in metastasis. In *Nature Reviews Cancer* (Vol. 5, Issue 10, pp. 786–795).
761 https://doi.org/10.1038/nrc1713
762 Chang, D. C., Xu, N., & Luo, K. Q. (2003). Degradation of cyclin B is required for the onset of
763 anaphase in mammalian cells. *Journal of Biological Chemistry*, *278*(39), 37865–37873.
764 https://doi.org/10.1074/jbc.M306376200
765 Chen, G., & Deng, X. (2018). Cell Synchronization by Double Thymidine Block. *Bio-Protocol*,
766 *8*(17). https://doi.org/10.21769/bioprotoc.2994

767 Choi, C. H., Webb, B. A., Chimenti, M. S., Jacobson, M. P., & Barber, D. L. (2013). Ph sensing
768 by FAK-His58 regulates focal adhesion remodeling. *Journal of Cell Biology*, *202*(6), 849–
769 859. https://doi.org/10.1083/jcb.201302131
770 Czowski, B. J., Romero-Moreno, R., Trull, K. J., & White, K. A. (2020). Cancer and pH dynamics:
771 Transcriptional regulation, proteostasis, and the need for new molecular tools. In *Cancers*
772 (Vol. 12, Issue 10, pp. 1–19). MDPI AG. https://doi.org/10.3390/cancers12102760
773 Dagogo-Jack, I., & Shaw, A. T. (2018). Tumour heterogeneity and resistance to cancer therapies.
774 In *Nature Reviews Clinical Oncology* (Vol. 15, Issue 2, pp. 81–94). Nature Publishing Group.
775 https://doi.org/10.1038/nrclinonc.2017.166
776 De Boer, L., Oakes, V., Beamish, H., Giles, N., Stevens, F., Somodevilla-Torres, M., DeSouza,
777 C., & Gabrielli, B. (2008). Cyclin A/cdk2 coordinates centrosomal and nuclear mitotic events.
778 *Oncogene*, *27*(31), 4261–4268. https://doi.org/10.1038/onc.2008.74
779 Deutsch, C., Taylor, J. S., & Wilson, D. F. (1982). Regulation of intracellular pH by human
780 peripheral blood lymphocytes as measured by 19F NMR. *Proceedings of the National*
781 *Academy of Sciences of the United States of America*, *79*(24 I), 7944–7948.
782 https://doi.org/10.1073/pnas.79.24.7944
783 Flinck, M., Kramer, S. H., & Pedersen, S. F. (2018). Roles of pH in control of cell proliferation.
784 *Acta Physiologica*, *223*(3), e13068. https://doi.org/10.1111/apha.13068
785 Flinck, Mette, Kramer, S. H., Schnipper, J., Andersen, A. P., & Pedersen, S. F. (2018). The acid-
786 base transport proteins NHE1 and NBCn1 regulate cell cycle progression in human breast
787 cancer cells. *Cell Cycle*, *17*(9), 1056–1067. https://doi.org/10.1080/15384101.2018.1464850
788 Foster, I. (2008). Cancer: A cell cycle defect. In *Radiography* (Vol. 14, Issue 2, pp. 144–149).
789 W.B. Saunders. https://doi.org/10.1016/j.radi.2006.12.001
790 Fuster, D., Moe, O. W., & Hilgemann, D. W. (2004). Lipid- and mechanosensitivities of
791 sodium/hydrogen exchangers analyzed by electrical methods. *Proceedings of the National*

Academy of Sciences of the United States of America, *101*(28), 10482–10487. https://doi.org/10.1073/pnas.0403930101

Gillies, R. J., & Deamer, D. W. (1979). Intracellular pH changes during the cell cycle inTetrahymena. *Journal of Cellular Physiology*, *100*(1), 23–31. https://doi.org/10.1002/jcp.1041000103

Greaves, M., & Maley, C. C. (2012). Clonal evolution in cancer. In *Nature* (Vol. 481, Issue 7381, pp. 306–313). https://doi.org/10.1038/nature10762

Grillo-Hill, B. K., Choi, C., Jimenez-Vidal, M., & Barber, D. L. (2015). Increased H+ efflux is sufficient to induce dysplasia and necessary for viability with oncogene expression. *ELife*, *2015*(4), 1–31. https://doi.org/10.7554/eLife.03270

Grillo-Hill, B. K., Webb, B. A., & Barber, D. L. (2014). Ratiometric Imaging of pH Probes. In *Methods in Cell Biology* (Vol. 123, pp. 429–448). https://doi.org/10.1016/B978-0-12-420138-5.00023-9

Hinohara, K., & Polyak, K. (2019). Intratumoral heterogeneity: more than just mutations. *Trends Cell Biol.*, *29*(7), 569–579. https://doi.org/10.1016/j.tcb.2019.03.003

Jones, M. C., Zha, J., & Humphries, M. J. (2019). Connections between the cell cycle, cell adhesion and the cytoskeleton. In *Philosophical Transactions of the Royal Society B: Biological Sciences* (Vol. 374, Issue 1779). Royal Society Publishing. https://doi.org/10.1098/rstb.2018.0227

Karagiannis, J., & Young, P. G. (2001). *Intracellular pH homeostasis during cell-cycle progression and growth state transition in Schizosaccharomyces pombe*. Journal of Cell Science. https://doi.org/https://doi.org/10.1242/jcs.114.16.2929

Korenchan, D. E., & Flavell, R. R. (2019). Spatiotemporal pH heterogeneity as a promoter of cancer progression and therapeutic resistance. In *Cancers* (Vol. 11, Issue 7, p. 1026). MDPI AG. https://doi.org/10.3390/cancers11071026

817 Lawson, D. A., Kessenbrock, K., Davis, R. T., Pervolarakis, N., & Werb, Z. (2018). Tumour
818 heterogeneity and metastasis at single-cell resolution. *Nature Cell Biology*, *20*(12), 1349–
819 1360. https://doi.org/10.1038/s41556-018-0236-7
820 Lee, A. H., & Tannock, I. F. (1998). Heterogeneity of intracellular pH and of mechanisms that
821 regulate intracellular pH in populations of cultured cells. *Cancer Research*, *58*(9), 1901–
822 1908.
823 Liu, M., Liu, H., & Chen, J. (2018). Mechanisms of the CDK4/6 inhibitor palbociclib (PD 0332991)
824 and its future application in cancer treatment (Review). In *Oncology Reports* (Vol. 39, Issue
825 3, pp. 901–911). Spandidos Publications. https://doi.org/10.3892/or.2018.6221
826 Lobo, R. C., Hubbard, N. E., Damonte, P., Mori, H., Pénzváltó, Z., Pham, C., Koehne, A. L., Go,
827 A. C., Anderson, S. E., Cala, P. M., & Borowsky, A. D. (2016). Glucose Uptake and
828 Intracellular pH in a Mouse Model of Ductal Carcinoma In situ (DCIS) Suggests Metabolic
829 Heterogeneity. *Frontiers in Cell and Developmental Biology*, *4*(AUG), 93.
830 https://doi.org/10.3389/fcell.2016.00093
831 Mirkka Koivusalo, Christopher Welch, Hisayoshi Hayashi, Cameron C. Scott, Moshe Kim, Todd
832 Alexander, Nicolas Touret, Klaus M. Hahn, and S. G. (2010). Amiloride inhibits
833 macropinocytosis by lowering submembranous pH and preventing Rac1 and Cdc42
834 signaling. *Journal of Cell Biology*. https://doi.org/10.1083/jcb.200908086
835 Putney, L. K., & Barber, D. L. (2003). Na-H Exchange-dependent Increase in Intracellular pH
836 Times G2/M Entry and Transition. *Journal of Biological Chemistry*, *278*(45), 44645–44649.
837 https://doi.org/10.1074/jbc.M308099200
838 Reshkin, S. J., Bellizzi, A., Caldeira, S., Albarani, V., Malanchi, I., Poignee, M., Alunni-Fabbroni,
839 M., Casavola, V., & Tommasino, M. (2000). Na + /H + exchanger-dependent intracellular
840 alkalinization is an early event in malignant transformation and plays an essential role in the
841 development of subsequent transformation-associated phenotypes. *The FASEB Journal*,
842 *14*(14), 2185–2197. https://doi.org/10.1096/fj.00-0029com

843 Saccomano, M., Alves, F., Swietach, P., Dovmark, T. H., & Hulikova, A. (2017). Connexin-43
844 channels are a pathway for discharging lactate from glycolytic pancreatic ductal
845 adenocarcinoma cells. *Oncogene*, *36*(32), 4538–4550. https://doi.org/10.1038/onc.2017.71
846 Sellier, C., Bodart, J. F., Flament, S., Baert, F., Cannon, J., & Vilain, J. P. (2006). Intracellular
847 acidification delays hormonal G2/M transition and inhibits G2/M transition triggered by
848 thiophosphorylated MAPK in xenopus oocytes. *Journal of Cellular Biochemistry*, *98*(2), 287–
849 300. https://doi.org/10.1002/jcb.20764
850 Sergeeva, T. F., Shirmanova, M. V., Zlobovskaya, O. A., Gavrina, A. I., Dudenkova, V. V., Lukina,
851 M. M., Lukyanov, K. A., & Zagaynova, E. V. (2017). Relationship between intracellular pH,
852 metabolic co-factors and caspase-3 activation in cancer cells during apoptosis. *Biochimica*
853 *et Biophysica Acta - Molecular Cell Research*, *1864*(3), 604–611.
854 https://doi.org/10.1016/j.bbamcr.2016.12.022
855 Siu, K. T., Rosner, M. R., & Minella, A. C. (2012). An integrated view of cyclin E function and
856 regulation. In *Cell Cycle* (Vol. 11, Issue 1, pp. 57–64). Taylor and Francis Inc.
857 https://doi.org/10.4161/cc.11.1.18775
858 Taubenberger, A. V., Baum, B., & Matthews, H. K. (2020). The Mechanics of Mitotic Cell
859 Rounding. In *Frontiers in Cell and Developmental Biology* (Vol. 8, p. 687). Frontiers Media
860 S.A. https://doi.org/10.3389/fcell.2020.00687
861 Taylor, I. W., & Hodson, P. J. (1984). Cell cycle regulation by environmental pH. *Journal of Cellular*
862 *Physiology*, *121*(3), 517–525. https://doi.org/10.1002/jcp.1041210310
863 Trotter, E. W., & Hagan, I. M. (2020). Release from cell cycle arrest with Cdk4/6 inhibitors
864 generates highly synchronised cell cycle progression in human cell culture. In *bioRxiv* (p.
865 2020.07.04.187625). bioRxiv. https://doi.org/10.1101/2020.07.04.187625
866 Webb, B. A., White, K. A., Grillo-Hill, B. K., Schönichen, A., Choi, C., & Barber, D. L. (2016). A
867 Histidine Cluster in the Cytoplasmic Domain of the Na-H Exchanger NHE1 Confers pH-

868 sensitive Phospholipid Binding and Regulates Transporter Activity *. *Journal of Biological*
869 *Chemistry*, *291*(46), 24096–24104. https://doi.org/10.1074/jbc.M116.736215
870 Weiß, I., & Bohrmann, J. (2019). Electrochemical gradients are involved in regulating cytoskeletal
871 patterns during epithelial morphogenesis in the Drosophila ovary. *BMC Developmental*
872 *Biology*, *19*(1). https://doi.org/10.1186/s12861-019-0203-y
873 White, K. A., Grillo-Hill, B. K., & Barber, D. L. (2017). Cancer cell behaviors mediated by
874 dysregulated pH dynamics at a glance. *Journal of Cell Science*, *130*, 663–669.
875 https://doi.org/10.1242/jcs.195297
876